Journal of Catalysis 257 (2008) 297–306

Contents lists available at ScienceDirect

Journal of Catalysis

www.elsevier.com/locate/jcat

Correlating hydrogenation activity with binding energies of hydrogen and cyclohexene on M/Pt(111) (M = Fe, Co, Ni, Cu) bimetallic surfaces

Michael P. Humbert, Jingguang G. Chen *

Department of Chemical Engineering, Center for Catalytic Science and Technology (CCST), University of Delaware, Newark, DE 19716, USA

ARTICLE INFO

Article history:
Received 14 March 2008
Revised 25 April 2008
Accepted 11 May 2008
Available online 18 June 2008

Keywords:
Platinum
Nickel
Cobalt
Iron
Copper
Bimetallic surfaces
Hydrogenation
Cyclohexene

ABSTRACT

This study used a combination of density functional theory (DFT) and temperature-programmed desorption (TPD) to determine trends in the hydrogenation activity of cyclohexene on several bimetallic surfaces prepared by modifying Pt(111) with 3d transition metals (Fe, Co, Ni, and Cu). The hydrogen binding energy (HBE) on the subsurface Pt-3d-Pt(111) "sandwich" structures was significantly lower than that on the corresponding 3d-Pt-Pt(111) surface structures and monometallic parent metal surfaces. The binding of cyclohexene on these surfaces followed the same trend as that of HBE. The weaker binding energies of atomic hydrogen and cyclohexene on Pt-3d-Pt(111) led to a novel low-temperature hydrogenation pathway that did not occur on either 3d-Pt-Pt(111) or the corresponding parent metal surfaces. Pt-Ni-Pt(111) had the highest hydrogenation activity among the surfaces studied, with 0.030 molecules of cyclohexene converted to cyclohexane per surface metal atom. This activity was maximized on the Pt-Ni-Pt(111) surface, which had an intermediate cyclohexene binding energy, leading to a volcano-type relationship between hydrogenation activity and cyclohexene binding energy.

1. Introduction

Many bimetallic catalysts have been shown to have catalytic properties that differ distinctly from those of their parent metals [1]. In many cases, these unique properties result in activities and/or selectivities that exceed those achievable with a monometallic catalyst. For this reason, there have been many fundamental experimental and theoretical studies of the novel properties of well-defined bimetallic surfaces [2–9].

To study the modification effects on surface chemistry due to bimetallic formation, a monolayer film of one metal can be deposited onto a single-crystal substrate of another metal. Lattice mismatch results in the contraction or expansion of adlayer metal–metal bond length compared with that of the bulk metal, leading to a modification of the surface electronic properties due to the strain effect [6,10,11]. In addition, the formation of heterometallic bonds further alters the electronic properties of the surface, which is often referred to as the ligand effect. One useful parameter to describe the changes in the electronic properties of bimetallic surfaces is the position of the surface d-band center with respect to the Fermi level [12]. This parameter has been shown to strongly correlate with the ability of bimetallic surfaces to bind with small adsorbates, such as atomic hydrogen and oxygen [13], alkenes [8,14], and oxygenates [15,16]. In addition, activation barriers to such reactions as ethylene and maleic anhydride hydrogenation also have been correlated with the surface d-band center [8,17]. Thus, its determination may enable first-principles predictions of bimetallic surfaces with desirable catalytic properties for reactions involving these molecules [18].

In the present work, a combination of density functional theory (DFT) modeling and surface science experiments was used to study the effects of bimetallic formation on the binding of atomic hydrogen and cyclohexene, as well as on the low-temperature hydrogenation of cyclohexene. This was done by modifying Pt(111) with several 3d transition metals, including Fe, Co, Ni, and Cu. Depositing these metals on a Pt(111) single-crystal surface at room temperature was found to result in the formation of a surface monolayer of the 3d metals; these surfaces are designated as 3d-Pt-Pt(111). At elevated temperatures, the formation of a surface alloy is observed for each Pt-3d pair [9,19–27]. These surface alloys have been shown to be enriched in Pt in the first atomic layer due to the enthalpic driving potential created by the lower surface energy of Pt compared with the 3d metals under consideration [28,29]. Strain also may play a part in the interdiffusion of the Pt and 3d metals, because elastic strain is reduced by having the larger Pt atoms in the topmost atomic layer [23]. These Pt-enriched bimetallic surfaces are designated Pt-3d-Pt(111) in this study. Kitchin et al. [28] studied Ni modification of Pt(111) and found that surface Ni shifts the surface d-band center closer to the Fermi level in comparison to Ni(111), whereas subsurface Ni in the second atomic layer moves the d-band center away from the Fermi

* Corresponding author.
E-mail address: jgchen@udel.edu (J.G. Chen).

0021-9517/$ – see front matter
doi:10.1016/j.jcat.2008.05.013

level. The current study extends these findings to Fe-, Co-, and Cu-modified Pt(111) surfaces.

Cyclohexene can undergo decomposition, dehydrogenation, and self-hydrogenation (disproportionation) reactions, as well as hydrogenation in the presence of co-adsorbed atomic hydrogen. Due to the competitive nature of these reaction pathways, it is an ideal probe molecule for comparing the general trends in the chemical properties of the various bimetallic surfaces. On Pt(111), cyclohexene undergoes dehydrogenation and decomposition [7,30]; however, when Pt(111) is modified with another metal, the dominant reaction pathways can vary markedly. For example, modification with Sn can promote reversible adsorption, making molecular desorption the dominant pathway. Previous studies on 3d-modified Pt(111) have shown that the subsurface Pt-Ni-Pt(111) and Pt-Co-Pt(111) structures exhibit a novel low-temperature hydrogenation pathway [28,31,32]. Similar results were observed in the current study for the Pt-Fe-Pt(111) surface; however, the Pt-Cu-Pt(111) surface did not exhibit the same hydrogenation pathway. Furthermore, the current study also investigated the hydrogenation pathway on the four 3d-Pt-Pt(111) surfaces and found that this pathway did not occur on these surface structures because of the strong binding of cyclohexene and atomic hydrogen. The combined experimental results and DFT modeling allow us to establish a volcano-type relationship between the binding energies and hydrogenation activities among the various 3d/Pt(111) bimetallic surfaces.

2. Experimental

2.1. Preparation of bimetallic surfaces

The current study was performed in a two-level stainless steel ultra-high vacuum (UHV) chamber with a base pressure of 1×10^{-10} Torr. This chamber was equipped with an Auger electron spectrometer (AES) with a single-pass cylindrical mirror analyzer for surface characterization and a quadrupole mass spectrometer (MS) for temperature-programmed desorption (TPD) experiments and *in-situ* verification of the purity of the dosed gases. A Pt(111) single-crystal disk (99.999%, Metal Crystals and Oxides, Ltd., Cambridge), measuring 12 mm in diameter and 1.5 mm in thickness, was spot-welded directly to two tantalum posts. The crystal could be resistively heated with a DC power supply to 1100 K or cooled with liquid nitrogen to 100 K. By spot welding a thermocouple to the back of the Pt(111) crystal, and connecting this signal to a feedback controller, the crystal temperature could be accurately monitored and controlled.

Before each experiment, the Pt(111) surface was cleaned by several Ne^+ sputter cycles at 600 K, with subsequent flashes to 1050 K. This was followed by oxygen dosing (1×10^{-8} Torr for 50 s) at 890 K and annealing at 1050 K for 5 min. The surface was then modified by depositing a 3d metal using physical vapor deposition. This was accomplished by wrapping a 0.1 mm diameter wire of the desired 3d metal around a 0.5 mm diameter tungsten wire, winding this into a filament, and enclosing the filament in a stainless steel shield to direct the 3d metal vapor onto the Pt(111) surface when the filament is resistively heated with a DC power supply. Tungsten and all 3d metal wires were purchased from Alfa Aesar, and were 99.95+% pure. When the temperature of the Pt(111) was maintained at 300 K during deposition, the 3d metal remained on the surface. On the other hand, if the crystal temperature was elevated to 600 K during deposition, then the 3d metal began to diffuse into the subsurface region, with the first atomic layer being enriched in Pt [19–27]. This was previously determined for the Ni/Pt(111) and Co/Pt(111) bimetallic surfaces [28,32].

The current study was extended to the growth and thermal behavior of Fe and Cu on the Pt(111) surface. The quantity of 3d metal deposited was determined by the 3d (LMM)/Pt (241 eV) AES peak-to-peak ratio, noting that an accelerating voltage of 3 kV was used in all AES measurements. Each surface was prepared with a coverage of approximately one monolayer (ML) of the respective 3d metal, which was deposited at a rate of 0.2–0.3 ML/min. Assuming a layer-by-layer growth mode, we would have expected to see clear breaks in the AES peak-to-peak heights of the Pt and 3d signals as a function of deposition time at the ML coverage. These breaks were observed for Ni, Co, and Fe deposition and to some extent with Cu deposition.

Fig. 1 displays the change in the Pt and Fe AES intensities, along with the ratio of the Fe to Pt intensities, as a function of time at an approximately constant deposition rate. A break in the Fe and Pt intensities at around 300 s is indicative of deposition of the first ML of Fe, at an Fe/Pt AES ratio of ~1.6. For the deposition of Cu (Fig. 2), a break in the Pt signal was evident, whereas breaks in the Cu signal were not easily seen. Based on the break in the

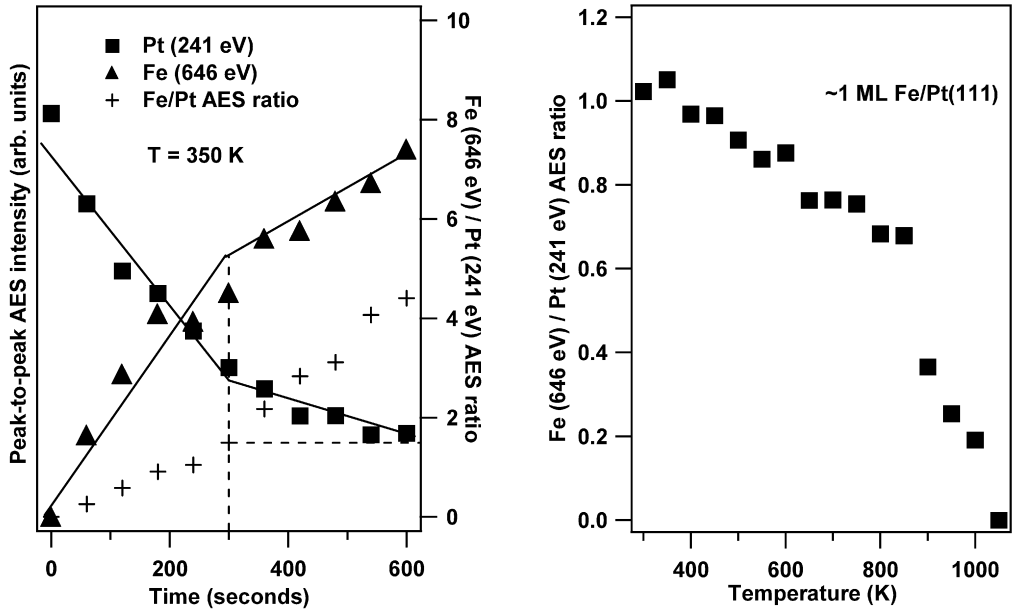

Fig. 1. AES quantification of the physical vapor deposition and thermal behavior of Fe on Pt(111).

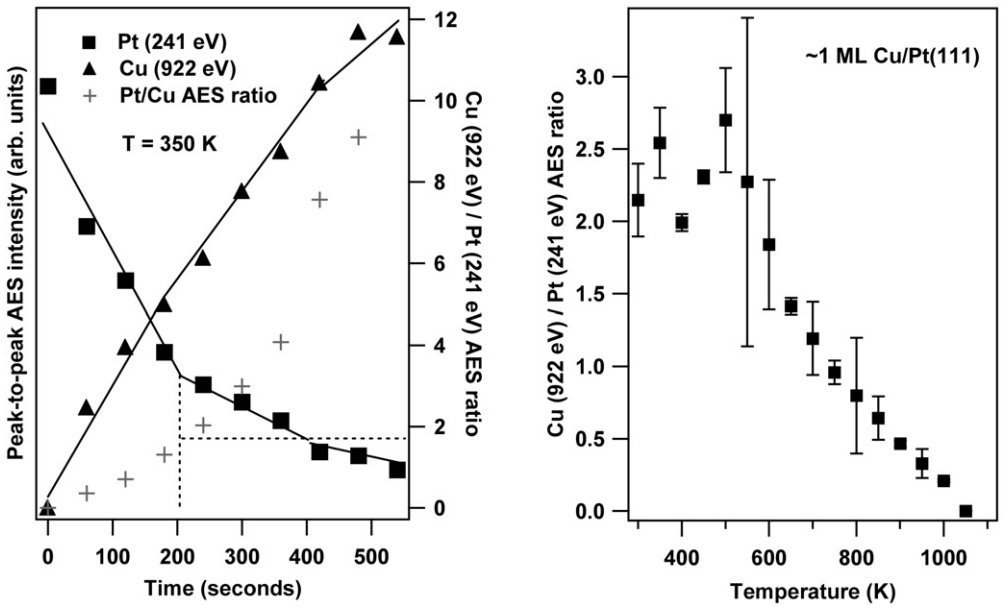

Fig. 2. AES quantification of the physical vapor deposition and thermal behavior of Cu on Pt(111).

Pt curve, a ML of Cu was deposited in 210 s; this corresponds to a Cu/Pt AES ratio of ∼1.8. The Fe/Pt and Cu/Pt AES ratios were supported by calculations in which values of the inelastic mean free path (IMFP) of the Auger electrons through the elements of interest were used [33]. Using a model of an atomically thin overlayer element (Fe or Cu) on a substrate (Pt), the calculated AES ratios were 1.7 for the Fe-Pt-Pt(111) surface and 1.8 for the Cu-Pt-Pt(111) surface, in general agreement with the experimental results.

Figs. 1 and 2 also show the thermal behavior of ∼1 ML of Fe and Cu on Pt(111). Each of these metals was deposited at 300 K. The surfaces were then heated at 3 K/s to increasingly high temperatures, and AES scans were performed once the surfaces were cooled to below 500 K, to determine changes in the surface composition. From Fig. 1, it is clear that the Fe/Pt AES ratio decreased steadily from 300 K up to ∼850 K, at which point it decreased abruptly. This is indicative of a gradual diffusion of Fe into the subsurface region between 300 and 850 K, with the diffusion of Fe into the bulk of Pt(111) at temperatures above 850 K. Given this evidence, deposition of Fe at 600 K, which is in the middle of this alloy formation region, was performed to create a Pt-Fe-Pt(111) surface. The ∼1 ML Cu surface exhibited similar behavior but with a less pronounced critical temperature above which rapid diffusion into the bulk occurred. The surface was relatively stable up to 550 K, after which the Cu/Pt ratio began to decrease steadily. For this reason, a temperature of 600 K also was used to create the Pt-Cu-Pt(111) surface alloy.

In summary, 3d-Pt-Pt(111), or the surface configuration, is representative of 1 ML of the 3d metal on Pt(111) and was prepared by depositing 1 ML at 300 K. This surface was modeled as one layer of 3d metal on top of bulk Pt(111). The subsurface bimetallic configuration, designated Pt-3d-Pt(111), was prepared by depositing 1 ML of the 3d metal at 600 K. This surface was modeled as bulk Pt(111) with the second atomic layer replaced by the 3d metal. The Ni and Co-modified Pt(111) surfaces were prepared in the same manner as the Fe and Cu-modified Pt(111) surfaces, using previously reported AES calibration curves [28,34]. The other surfaces used in the current study were pseudomorphic films of Fe, Co, Ni and Cu, for which approximately five to ten monolayers of the 3d metal were deposited on Pt(111) such that Pt was barely detectable in the AES scan. The thin film surfaces were modeled as the bulk closed packed 3d surface for each respective metal.

2.2. TPD measurements

After the bimetallic surfaces were synthesized, hydrogen (Matheson, 99.999%) and cyclohexene (c-C_6H_{10}) (Aldrich, 99+%) were dosed on the surfaces at <150 K and <130 K, respectively. Cyclohexene was purified by successive freeze–pump–thaw cycles before use. Hydrogen, along with neon and oxygen, were of research-grade purity (99.999%) and were introduced into the UHV chamber without further purification. For the H_2 TPD experiments, the hydrogen dose was 5 L for the Ni, Fe, and Cu surfaces and 10 L for the Co surfaces. The coverage of predosed hydrogen for the cyclohexene hydrogenation studies was approximately 40–50% of the saturation coverage, as determined by an exposure series on Pt(111) and assuming a similar sticking coefficient on each surface studied. The cyclohexene exposure was 2 L for all surfaces, an amount that provided significant coverage with no appreciable multilayer formation. Cyclohexene and neon were backfilled into the chamber through leak valves, whereas hydrogen and oxygen were dosed through directional dosing tubes approximately 8 mm in diameter. After dosing, the surface was placed ∼5 mm from the opening of the random flux shield of the MS. TPD experiments were then performed with a linear heating rate of 3 K/s, with up to 10 masses monitored simultaneously.

2.3. DFT modeling

DFT was used to calculate the binding energies of atomic hydrogen and cyclohexene on the monometallic and bimetallic surfaces. The theoretical results presented in this paper were calculated using self-consistent periodic slab calculations with the VASP (Vienna *ab initio* Simulation Package) code [35–37]. The Kohn Sham equations were solved using a plane-wave basis set with a cutoff energy of 396 eV, and the PW91 functional was used to describe the exchange correlation term. Vanderbilt ultrasoft pseudopotentials, as supplied by G. Kresse and J. Hafner, were used to describe the core electrons and the nuclei of the atoms [38,39]. A $3 \times 3 \times 1$ Monkhorst-pack *k*-point grid mesh was used to determine the electronic energies. The d-band center was calculated by projecting the plane waves onto spherical harmonic orbitals using the Dacapo v2.7 code [40]. The d-band center in the current study is defined as the first moment of the d-orbital states for the surface atoms

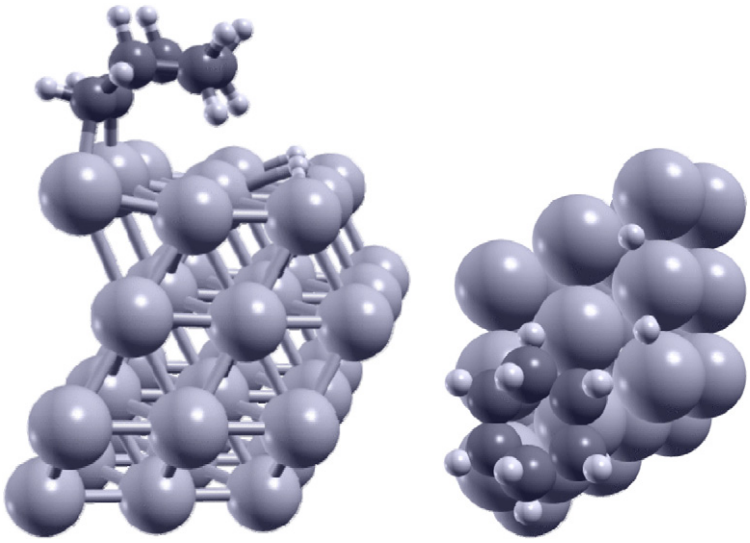

(a) (b)

Fig. 3. Bonding configuration of coadsorbed hydrogen and cyclohexene on Pt(111) as determined by DFT modeling. (a) Side view at approximately 30° from the normal; (b) top view.

using a Gaussian smearing method between k points and an infinite cutoff radius.

The binding energies of atomic hydrogen and cyclohexene were studied using 3×3 super cells containing four atomic layers, with the top two layers allowed to relax in each case. A vacuum region of about six metal layers was used to separate the slabs, to avoid any electronic interactions. Calculations for gas-phase hydrogen and cyclohexene were carried out implementing spin-polarization, whereas the adsorbate–metal system calculations were carried out spin-unpolarized, because the relative difference in the adsorption energies with and without spin-polarization was typically found to be <5 kJ/mol for atomic hydrogen and alkenes [28,41].

For the hydrogen–metal system, hydrogen was adsorbed in the threefold hollow site of the metal surface with a coverage of 1/9 ML. The adsorbate–slab system was then allowed to relax to its minimum energy configuration. The binding energy was calculated as the difference between the adsorbate–slab total energy and the sum of the total energy of gas-phase adsorbate and the bare slab. The binding of cyclohexene was studied on hydrogen co-adsorbed surfaces. One cyclohexene molecule was bonded in the di-σ configuration on the monometallic and bimetallic surfaces, with the presence of two co-adsorbed hydrogen atoms in the 3×3 super cell. The hydrogen atoms were bonded in the two threefold hollow sites nearest to the cyclohexene molecule, to ascertain the effect of repulsion on the binding of cyclohexene. Fig. 3 shows the bonding configuration of co-adsorbed cyclohexene and hydrogen on the Pt(111) surface. The binding energies of both the boat and chair configurations were calculated, demonstrating that the boat configuration is the thermodynamically preferred structure for di-σ bonded cyclohexene.

3. Results and discussion

3.1. Validity of Pt-3d-Pt(111) and 3d-Pt-Pt(111) model surfaces

Naturally, the model surfaces in this study are approximations to the actual surfaces. Although the deposition of 3d metals on Pt(111) at 300 K appears to follow the layer-by-layer growth mechanism, as indicated by the distinct breaks in Figs. 1 and 2 for Fe and Cu deposition and in previously published AES calibration curves for Ni and Co deposition, a fraction of 3d atoms likely will form a second layer prior to the completion of the first monolayer.

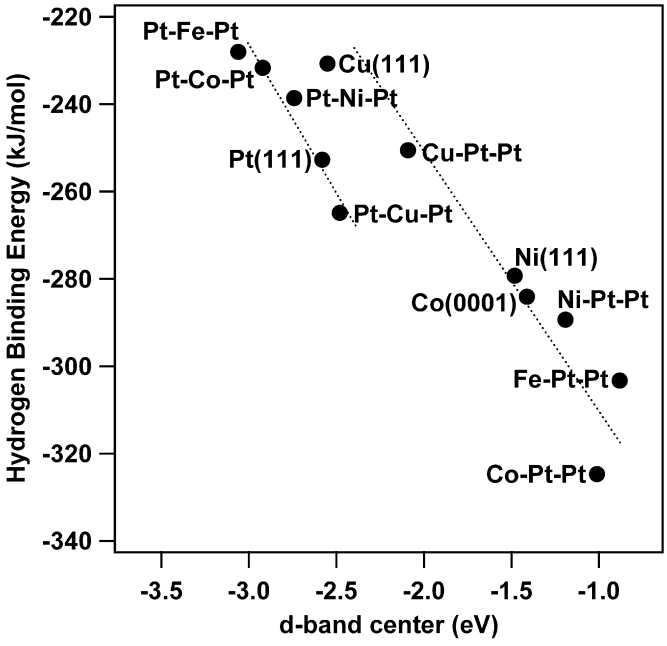

Fig. 4. Correlation between HBE and d-band center of bimetallic surfaces as determined by DFT.

In addition, deposition at the elevated temperature of 600 K leads to the diffusion of 3d metals into the subsurface region, but the composition of each layer is not exactly the ideal Pt-3d-Pt(111) structure. For example, in surface alloys formed by annealing a surface monolayer of 3d metal deposited onto Pt(111), the Pt composition at the first atomic layer and that of the 3d metal in the second atomic layer are typically 80% for Co and Ni bimetallic surfaces [26,28,32]. Despite this finding, Kitchin et al. [28] have reported a linear trend in the surface d-band centers of Pt-Ni-Pt(111), Pt(111), and Ni-Pt-Pt(111), where the presence of surface Ni atoms shifts the d-band center closer to the Fermi level and subsurface Ni atoms lead to the opposite shift in this parameter [28]. Thus, the model surfaces in the current study should be sufficient for qualitatively predicting the general trends among the

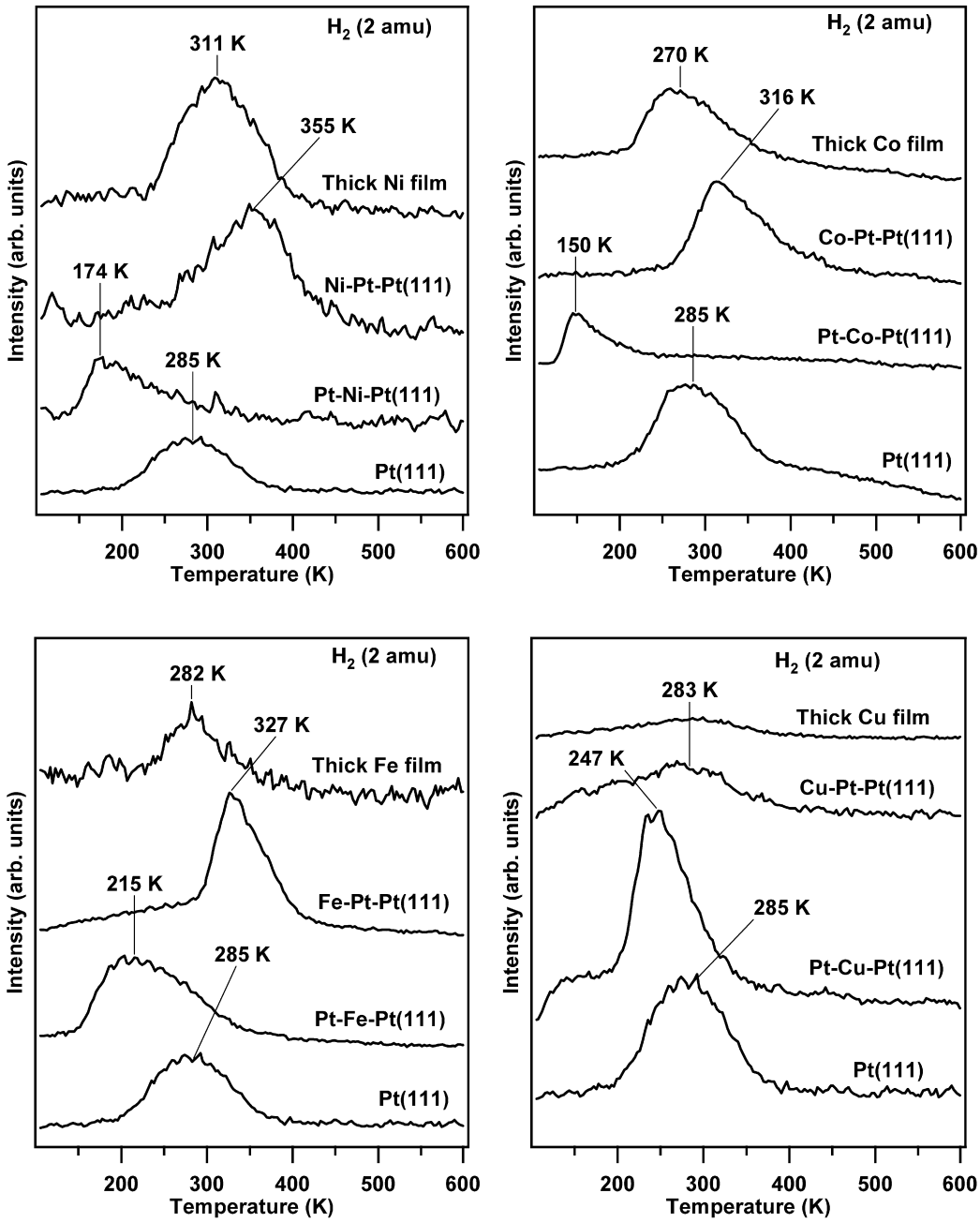

Fig. 5. TPD of hydrogen desorption from monometallic and bimetallic surfaces.

subsurface Pt-3d-Pt(111) and surface 3d-Pt-Pt(111) bimetallic structures.

Based on literature results and as confirmed by AES measurements, the Cu/Pt(111) surfaces prepared at 600 K in the current study should have a $Cu_{50}Pt_{50}$ stoichiometry and be confined to the first two atomic layers [24,25]. In addition, several different active sites are available on the Cu-Pt alloy due to its relative amount of disorder. Thus, the Cu/Pt(111) system differs greatly from the idealized Pt-Cu-Pt(111) model surface, and the trends in the binding energies are expected to differ from those on the other 3d/Pt(111) surfaces. As we show later, the idealized Pt-3d-Pt(111) and 3d-Pt-Pt(111) models are sufficient for correlating experimental and DFT results on the bimetallic surfaces, with the possible exception of the Cu/Pt(111) surfaces.

3.2. Trends in hydrogen binding energy (HBE)

DFT was used to estimate HBE on the model monometallic and bimetallic surfaces. Fig. 4 shows that the HBE values were predicted to increase as the d-band center moved closer to the Fermi level, in agreement with trends for other surfaces noted in previous studies [13,28,42]. Shown are two separate linear trends, one trend for surfaces terminated by 3d metals and the other for surfaces terminated by Pt. This arose due the difference in coupling between the adsorbates and the 3d and 5d surface metals, respectively, as discussed by Hammer and Norskov [12]. In general, adding the late transition 3d metals considered in this study to the surface of Pt(111) moved the d-band center closer to the Fermi level as compared with the bulk 3d metals. This resulted primarily from the tensile strain induced by the Pt lattice, because the

ligand effect was weakest between the late transition metal overlayer and the Pt(111) substrate. Conversely, subsurface 3d metals shifted the surface d-band center of Pt away from the Fermi level compared with that of Pt(111), due mainly to the electronic interaction of Pt and the subsurface 3d atoms [13]. The Cu/Pt(111) bimetallic surfaces appeared to show anomalous results compared with the general trends for the other surfaces; specifically, the surface and subsurface configurations of Cu/Pt(111) did not follow the same trend in binding energy as the other three 3d/Pt(111) bimetallic surfaces, with Pt-Cu-Pt(111) having a stronger HBE and Cu-Pt-Pt(111) having a weaker HBE compared with Pt(111). The anomalous behavior of Cu/Pt(111) surfaces is further evidenced by the fact that dissociative adsorption of hydrogen is reported to be activated on Cu(111) and on the surface Cu sites of the Cu/Pt(111) bimetallic surfaces [42]. These unique properties may be due to the fact that Cu has a filled d-band and only one valence s electron, and thus should interact with Pt(111) differently than the other 3d metals.

Fig. 5 compares these DFT trends with TPD results of hydrogen adsorption on the different 3d/Pt(111) bimetallic surfaces. Consistent with the DFT predictions, the subsurface Pt-3d-Pt(111) structures had lower desorption temperatures compared with the corresponding parent metals. The surface 3d-Pt-Pt(111) structures promoted a stronger metal–hydrogen bond, as indicated by higher desorption temperatures than seen for the corresponding parent metals. The behavior of the Cu/Pt(111) surfaces appears to be different from that of the other 3d/Pt(111) surfaces. H_2 desorbed from thick Cu at similar temperatures as Pt(111), but the peak was quite small, likely due to the activation of hydrogen adsorption on surface Cu atoms [42]. In fact, this peak may be due to hydrogen adsorption on the small number of surface Pt sites, on which adsorption was not activated.

Assuming that the dissociative adsorption of hydrogen is an unactivated process, the desorption temperature of H_2 should be related to the value of HBE on different surfaces [28]. As summarized in Fig. 6, the surfaces with the lowest HBE were Pt-Co-Pt(111), with a desorption temperature of 150 K, and Pt-Ni-Pt(111), with a desorption temperature of 174 K. In comparison, Ni-Pt-Pt(111), Fe-Pt-Pt(111), and Co-Pt-Pt(111) surfaces have hydrogen desorption temperatures of 355 K, 327 K, and 316 K, respectively. Comparing the DFT predictions in Fig. 4 with the H_2 desorption temperatures in Fig. 6 shows a general agreement between the modeling and experimental results. Thus, should HBE be a good indicator of reactivity; DFT could be used to predict bimetallic surfaces with desirable HBE values for specific catalytic reactions, such as the hydrogenation reaction described next.

3.3. Trends in hydrogenation activity

Cyclohexene was used as a chemical probe to determine the hydrogenation activity on these bimetallic surfaces. Because extensive characterization was performed on Ni/Pt(111) bimetallic surfaces, we first discuss the interaction of cyclohexene with these surfaces. Hwu et al. [31] performed high-resolution electron energy loss spectroscopy (HREELS) to determine the bonding orientation of cyclohexene and its intermediates and found that cyclohexene is di-σ-bonded to Pt(111) and thick Ni film, but only weakly π-bonded on Pt-Ni-Pt(111). Although that study did not examine cyclohexene adsorption on Ni-Pt-Pt(111), the bonding of cyclohexene on this surface can be elucidated by DFT modeling and TPD results. Table 1 gives the DFT results of cyclohexene binding on 3d/Pt(111) bimetallic surfaces under conditions of hydrogen and cyclohexene co-adsorption. The binding energies calculated in this work are in agreement with those given in the literature [7,43]. These results support the conclusions of Hwu et al. that cyclohexene is strongly bonded to Pt(111) and Ni(111) and more weakly bonded to Pt-Ni-Pt(111). In addition, DFT results show that cyclohexene is bonded more strongly to Ni-Pt-Pt(111) compared with the monometallic surfaces.

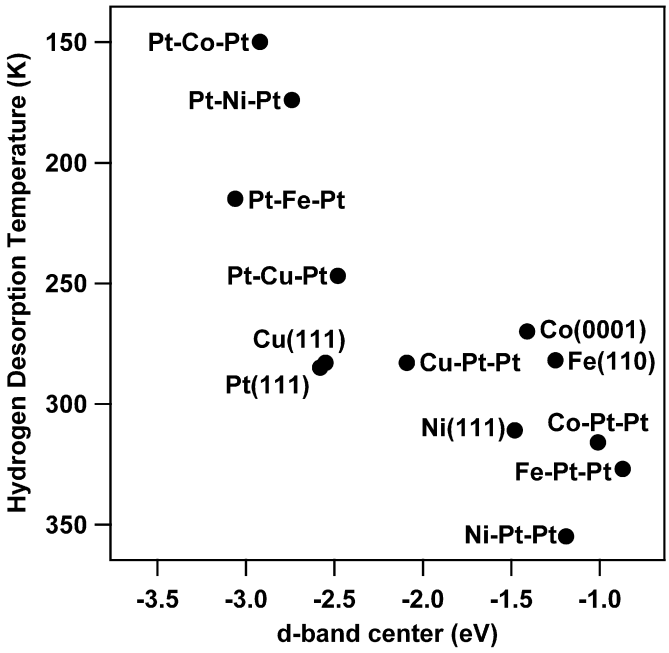

Fig. 6. Hydrogen desorption peak temperatures as a function of d-band center.

Table 1
DFT predicted cyclohexene binding energy on 3d/Pt(111) surfaces

Surface	d-band center (eV)	c-C_6H_{10} BE (kJ/mol)
Pt-Fe-Pt(111)	−3.06	−10.8
Pt-Co-Pt(111)	−2.92	−15.7
Cu-Pt-Pt(111)	−2.09	−20.4
Pt-Ni-Pt(111)	−2.74	−32.9
Ni(111)	−1.48	−52.0
Pt-Cu-Pt(111)	−2.48	−54.8
Pt(111)	−2.58	−69.6
Ni-Pt-Pt(111)	−1.19	−76.5
Co-Pt-Pt(111)	−1.01	−153.7
Fe-Pt-Pt(111)	−0.88	−161.3

Table 2
Cyclohexene hydrogenation and dehydrogenation activities on Pt-3d-Pt(111) surfaces

Surface	Activity (molecules/Pt atom)	
	C_6H_6	c-C_6H_{12}
Pt-Ni-Pt(111)	0.031	0.030
Pt-Co-Pt(111)	0.026	0.006
Pt-Fe-Pt(111)	0.030	0.005
Pt(111)	0.004	0.001
Pt-Cu-Pt(111)	0.007	0.000

Similar to the trend between the subsurface and surface Ni/Pt(111) structures, our DFT results predicted that the binding energy of cyclohexene follows the trend of Pt-Fe-Pt(111) < Pt(111) < Fe-Pt-Pt(111). Fig. 7 shows the corresponding TPD results after cyclohexene was dosed on the Fe/Pt(111) surfaces with pre-adsorbed hydrogen. The most interesting feature of these TPD experiments is the low-temperature hydrogenation pathway on Pt-Fe-Pt(111), which was significantly enhanced compared with the same surface without pre-adsorbed hydrogen (spectrum not shown). In contrast, this low-temperature hydrogenation pathway occurred only in trace amounts on Pt(111), Fe-Pt-Pt(111), and thick Fe film. The absence of the hydrogenation pathway on these surfaces is most likely due to the strong bonding of hydrogen and

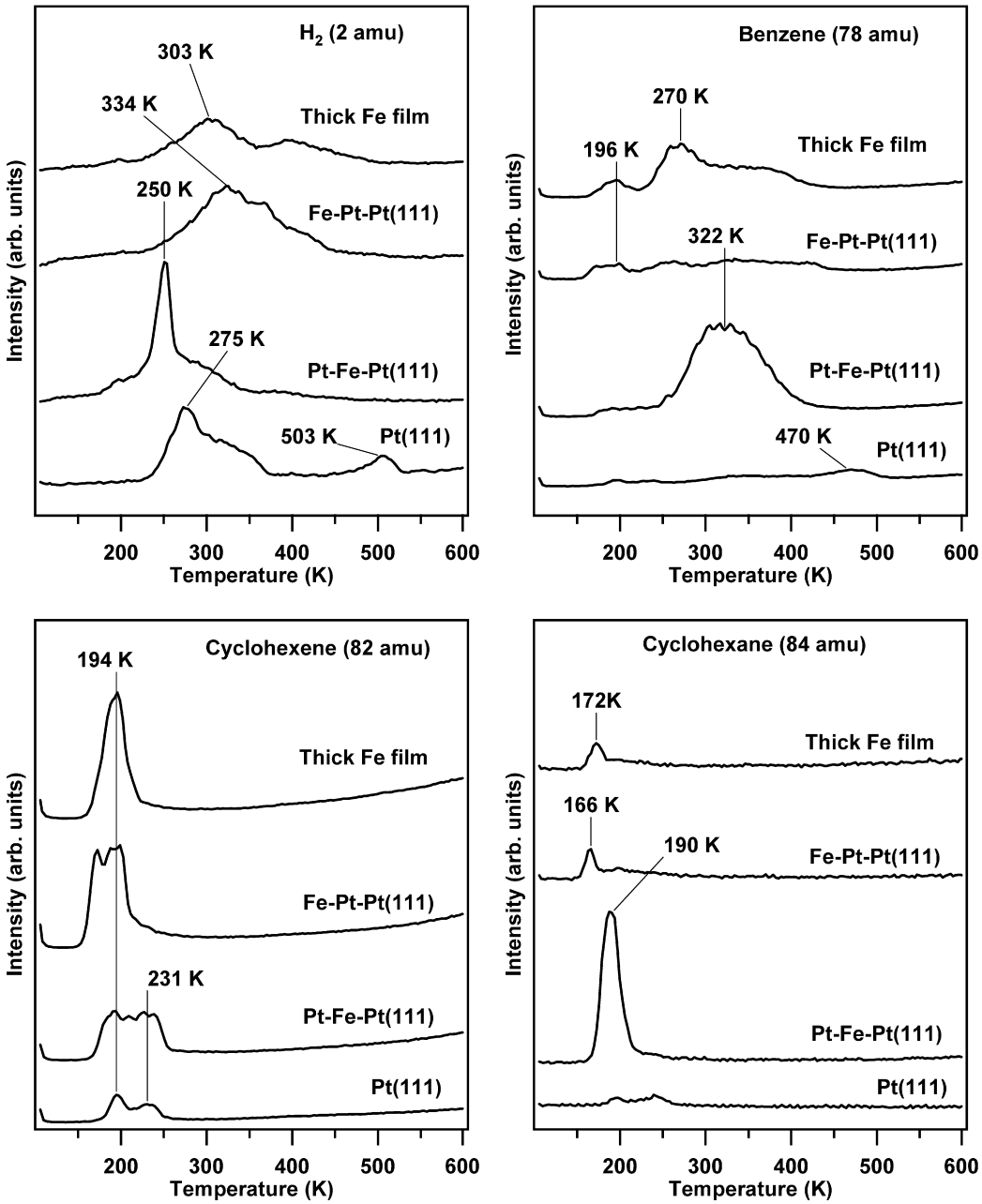

Fig. 7. TPD of cyclohexene on hydrogen pre-dosed Fe/Pt(111) surfaces.

cyclohexene, as predicted by DFT in Fig. 4 and Table 1, respectively.

Other reaction pathways, such as dehydrogenation to benzene, may be affected by the availability of surface sites on desorption of hydrogen. Rodriguez and Campbell [30] argued that the dehydrogenation of cyclohexene to benzene is limited by the number of free sites available to abstract hydrogen. Thus, increased benzene formation would be expected when hydrogen desorption precedes cyclohexene desorption. This is indeed seen on the Fe/Pt(111) surfaces. Fig. 7 shows that cyclohexene molecularly desorbs before hydrogen on Fe-Pt-Pt(111) and thick Fe. Correspondingly, only small amounts of benzene are produced on either of these surfaces. In contrast, hydrogen desorbs at lower temperatures on Pt-Fe-Pt(111), creating free sites before the molecular desorption of cyclohexene and leading to significant activity for the formation of benzene.

The H_2 peaks in Fig. 7 result from either the pre-adsorbed hydrogen or cyclohexene reacting on the surfaces. Fig. 5 showed that hydrogen desorbs from Fe-Pt-Pt(111) at 327 K. The fact that hydrogen is produced from this surface at higher temperatures (410 K) despite the lack of dehydrogenated products, such as benzene, is indicative of complete decomposition to atomic carbon and hydrogen. The observation of complete decomposition of cyclohexene on this surface supports the DFT prediction of strong cyclohexene bonding to the Fe-Pt-Pt(111) surface given in Table 1. It can be argued that decomposition is not a major pathway on the other Fe/Pt(111) surfaces, because the hydrogen produced on Pt-Fe-Pt(111) is likely due to benzene formation. Moreover, little hydrogen is produced on thick Fe, and any hydrogen that is produced evolves at similar temperatures as for benzene formation.

Similar TPD experiments on cyclohexene with pre-adsorbed hydrogen were performed on the Ni/Pt(111), Co/Pt(111), and Cu/Pt(111) surfaces. For the Ni- and Co-modified Pt(111) surfaces, the TPD results show the same trends as for the corresponding Fe/Pt(111) surfaces and are not shown here because most of those

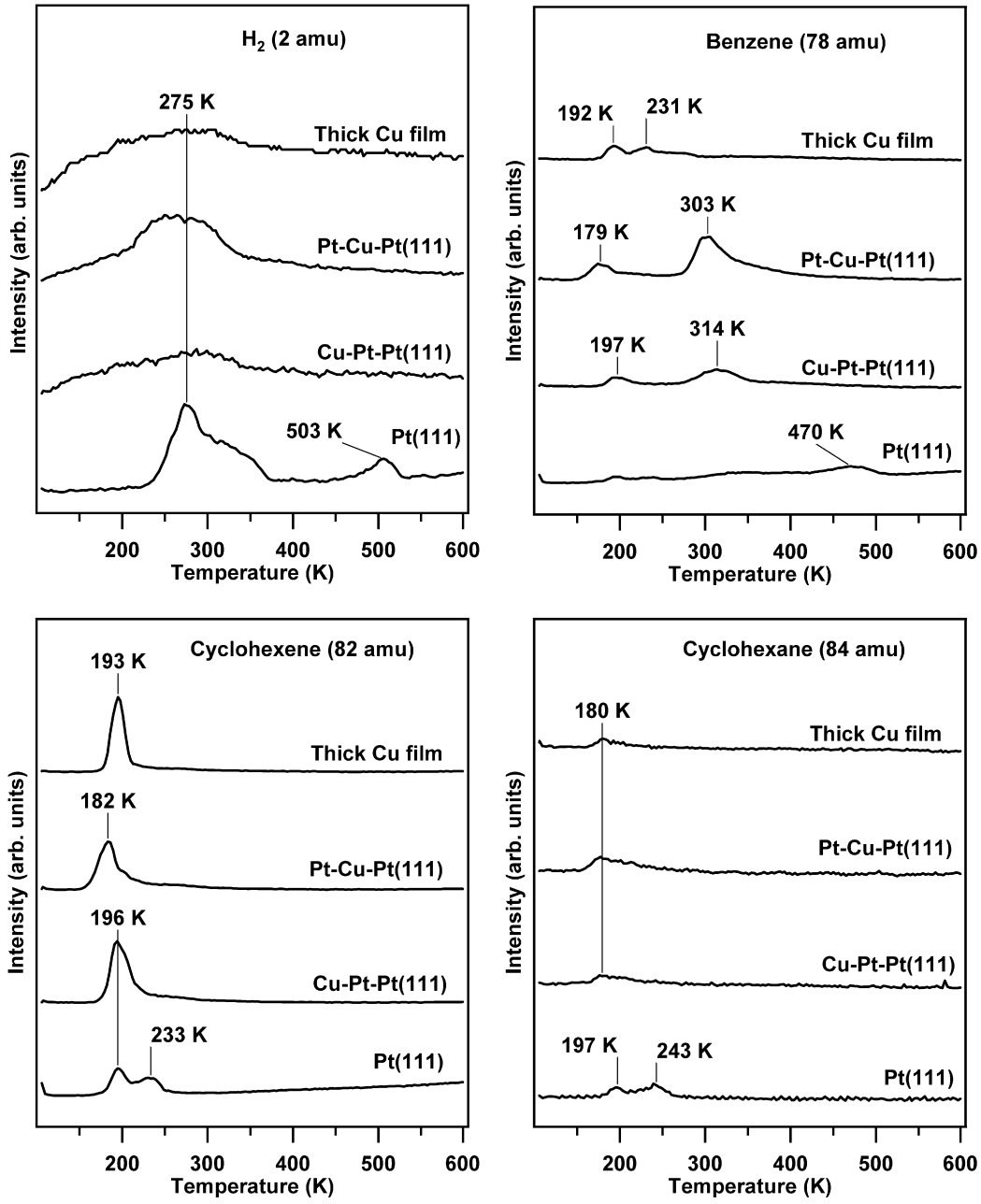

Fig. 8. TPD of cyclohexene on hydrogen pre-dosed Cu/Pt(111) surfaces.

results have been published previously [28,31,32]. In contrast, the Cu/Pt(111) surfaces do not follow this general trend. As shown in Fig. 8, these surfaces are largely inactive for all of the cyclohexene reaction pathways, with the predominant product being the molecular desorption of cyclohexene. The one exception is Pt-Cu-Pt(111), which produces a moderate amount of benzene.

Because the subsurface Pt-3d-Pt(111) structures have the most interesting hydrogenation and dehydrogenation properties, the results from each of these surfaces are compared in Fig. 9 and summarized in Table 2. The activities in Table 2 are quantified by TPD peak area ratios in conjunction with the following net reactions occurring on these surfaces:

$$x\mathrm{C_6H_{10}} \xrightarrow{\Delta} 6x\mathrm{C_{(ads)}} + 5x\mathrm{H_2}, \tag{1}$$

$$y\mathrm{C_6H_{10}} \xrightarrow{\Delta} y\mathrm{C_6H_6} + 2y\mathrm{H_2}, \tag{2}$$

and

$$z\mathrm{C_6H_{10}} + z\mathrm{H_2} \xrightarrow{\Delta} z\mathrm{C_6H_{12}}, \tag{3}$$

where x, y, and z represent the number of cyclohexene molecules in each respective reaction pathway. Because the activities on Pt-Ni-Pt(111) are known [34], TPD peak area ratios can be used to determine the activities of the other surfaces. The following equation is used to calculate benzene activity:

$$y_{\text{Pt-3d-Pt(111)}} = y_{\text{Pt-Ni-Pt(111)}} \frac{\text{area}^{\text{Pt-3d-Pt(111)}}_{\text{benzene}}}{\text{area}^{\text{Pt-Ni-Pt(111)}}_{\text{benzene}}}. \tag{4}$$

In this case, the activity toward the formation of benzene on Pt-3d-Pt(111) is calculated. The activity for cyclohexane formation is determined in exactly the same way, but using cyclohexane peak area ratios. Unfortunately, activity toward the decomposition pathway cannot be quantified using hydrogen peak areas because the

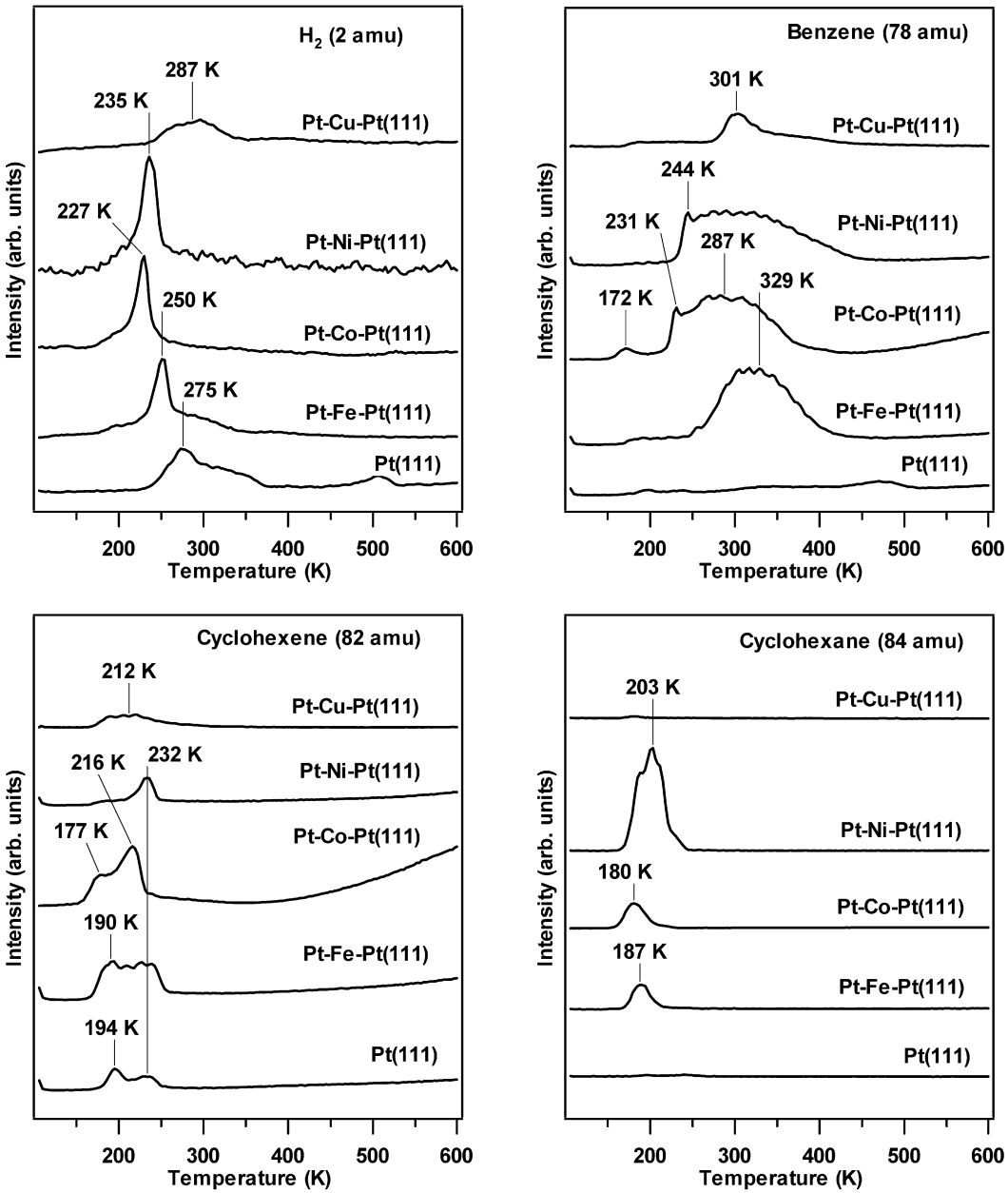

Fig. 9. Comparison of TPD results of cyclohexene on hydrogen pre-dosed Pt-3d-Pt(111) subsurface structures.

hydrogen evolved from the surface originates both from the dehydrogenation reactions and from the pre-adsorbed hydrogen. It is important to note that contributions from the cracking patterns of cyclohexene are subtracted during quantification of these activities. In addition, it is assumed that the density of surface sites of the Pt-3d-Pt(111) and 3d-Pt-Pt(111) bimetallic surfaces is similar to that of Pt(111).

From this quantification, it is evident that lower HBE generally results in higher hydrogenation activity. Pt-Co-Pt(111) deviates from this trend as it has the lowest HBE, but this does not lead to the highest hydrogenation activity. Of course, the assumption that HBE is the only factor governing hydrogenation activity is incorrect, because it does not consider the orientation or binding energy of cyclohexene on the surface. If cyclohexene binds too weakly, then it will molecularly desorb before any reaction can occur. Comparing Pt-Co-Pt(111) with Pt-Ni-Pt(111), DFT predicts that cyclohexene will bind very weakly to Pt-Co-Pt(111) compared with Pt-Ni-Pt(111) (Table 1). Thus, the hydrogenation activity appears to be maximized at an intermediate cyclohexene bond strength. This is clearly evident in Fig. 10, which shows the hydrogenation activity as a function of cyclohexene binding energy. The data points in Fig. 10 also include the binding energy and hydrogenation activity from a monolayer of Pt on a W(110) substrate, as reported previously [44]. These results clearly show that the subsurface Pt-3d-Pt(111) structures are preferred over 3d-Pt-Pt(111) for hydrogenation reactions. Because these surfaces have been found to be thermodynamically stable under vacuum and in the presence of hydrogen [13], the results of the current study should be directly applicable to more realistic catalytic hydrogenation conditions.

4. Conclusion

Our DFT results predict that surface 3d metals on Pt(111) will shift the surface d-band center closer to the Fermi level compared with the close-packed surfaces of the 3d metals. In contrast, incorporation of subsurface 3d metals will shift the d-band center away

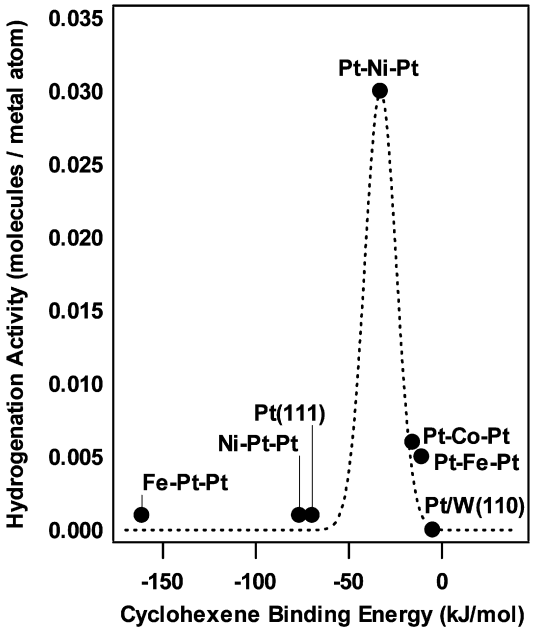

Fig. 10. Correlation of hydrogenation activity with the theoretically determined binding energy of cyclohexene.

from the Fermi level. A strong correlation between the position of the d-band center and the binding energies of atomic hydrogen and cyclohexene was evident. The DFT calculations predict that the Pt-3d-Pt(111) subsurface structures should have weaker HBE than both the corresponding 3d-Pt-Pt(111) surface structures and the parent metals. This prediction was verified by our TPD experiments. In addition, the Pt-3d-Pt(111) subsurface structures exhibited a low-temperature hydrogenation pathway not present on 3d-Pt-Pt(111) or the parent metal surfaces. This can be explained by the relatively weaker binding energies of atomic hydrogen and cyclohexene on the subsurface structures. Furthermore, a volcano-type relationship was found between the hydrogenation activity and binding energy of cyclohexene, with Pt-Ni-Pt(111) exhibiting the greatest activity. The Cu/Pt(111) surfaces did not follow the trends of the other 3d/Pt(111) surfaces in either the DFT modeling or TPD experiments, which can be partially explained by activation of H_2 dissociation on the Cu surfaces.

Acknowledgments

This work was supported by the U.S. Department of Energy, Office of Basic Energy Sciences (grant DE-FG02-00ER15104). The authors thank Amit Goda for his assistance with the DFT calculations.

References

[1] J.H. Sinfelt, Bimetallic Catalysts: Discoveries, Concepts, and Applications, John Wiley & Sons, New York, 1983.
[2] J.A. Rodriguez, Surf. Sci. Rep. 24 (1996) 225.
[3] J.A. Rodriguez, D.W. Goodman, Science 257 (1992) 897.
[4] A. Niquille-Rothlisberger, R. Prins, J. Catal. 242 (2006) 207.
[5] J.M. Heitzinger, S.C. Gebhard, B.E. Koel, J. Phys. Chem. 97 (1993) 5327.
[6] J.C. Bertolini, Appl. Catal. A Gen. 191 (2000) 15.
[7] F. Delbecq, F. Vigne-Maeder, C. Becker, J. Breitbach, K. Wandelt, J. Phys. Chem. C 112 (2008) 555.
[8] V. Pallassana, M. Neurock, J. Catal. 191 (2000) 301.
[9] J. Massardier, J.C. Bertolini, J. Catal. 90 (1984) 358.
[10] J.R. Kitchin, J.K. Norskov, M.A. Barteau, J.G. Chen, Phys. Rev. Lett. 93 (2004) 156801.
[11] M. Mavrikakis, B. Hammer, J.K. Norskov, Phys. Rev. Lett. 81 (1998) 2819.
[12] B. Hammer, J.K. Norskov, Adv. Catal. 45 (2000) 71.
[13] J.R. Kitchin, J.K. Norskov, M.A. Barteau, J.G. Chen, J. Chem. Phys. 120 (2004) 10240.
[14] M.B. Zellner, A.M. Goda, O. Skoplyak, M.A. Barteau, J.G. Chen, Surf. Sci. 583 (2005) 281.
[15] O. Skoplyak, M.A. Barteau, J.G. Chen, J. Phys. Chem. B 110 (2006) 1686.
[16] O. Skoplyak, C.A. Menning, M.A. Barteau, J.G. Chen, J. Chem. Phys. 127 (2007) 114707.
[17] V. Pallassana, M. Neurock, J. Phys. Chem. B 104 (2000) 9449.
[18] J.G. Chen, C.A. Menning, M.B. Zellner, Surf. Sci. Rep. 63 (2008) 201.
[19] P. Gambardella, K. Kern, Surf. Sci. 475 (2001) L229.
[20] C.W. Su, H.Y. Ho, C.S. Shern, R.H. Chen, Surf. Sci. 499 (2002) 103.
[21] V. Stamenkovic, T.J. Schmidt, P.N. Ross, N.M. Markovic, J. Electroanal. Chem. 554 (2003) 191.
[22] T.Y. Lee, S. Sarbach, K. Kuhnke, K. Kern, Surf. Sci. 600 (2006) 3266.
[23] C. Creemers, P. Deurinck, Surf. Interface Anal. 25 (1997) 177.
[24] N.T. Barrett, R. Belkhou, J. Thiele, C. Guillot, Surf. Sci. 333 (1995) 776.
[25] J.S. Tsay, T. Mangen, K. Wandelt, Thin Solid Films 397 (2001) 152.
[26] A. Atrei, U. Bardi, M. Galeotti, G. Rovida, M. Torrini, E. Zanazzi, Surf. Sci. 339 (1995) 323.
[27] D.I. Jerdev, B.E. Koel, Surf. Sci. 513 (2002) L391.
[28] J.R. Kitchin, N.A. Khan, M.A. Barteau, J.G. Chen, B. Yakshinksiy, T.E. Madey, Surf. Sci. 544 (2003) 295.
[29] C.A. Menning, H.H. Hwu, J.G.G. Chen, J. Phys. Chem. B 110 (2006) 15471.
[30] J.A. Rodriguez, C.T. Campbell, J. Catal. 115 (1989) 500.
[31] H.H. Hwu, J. Eng Jr., J.G. Chen, J. Am. Chem. Soc. 124 (2002) 702.
[32] N.A. Khan, L.E. Murillo, J.G. Chen, J. Phys. Chem. B 108 (2004) 15748.
[33] P.J. Cumpson, M.P. Seah, Surf. Interface Anal. 25 (1997) 430.
[34] N.A. Khan, M.B. Zellner, L.E. Murillo, J.G. Chen, Catal. Lett. 95 (2004) 1.
[35] G. Kresse, J. Hafner, Phys. Rev. B 47 (1993) 558.
[36] G. Kresse, J. Furthmuller, Comput. Mater. Sci. 6 (1996) 15.
[37] G. Kresse, J. Furthmuller, Phys. Rev. B 54 (1996) 11169.
[38] D. Vanderbilt, Phys. Rev. B 41 (1990) 7892.
[39] G. Kresse, J. Hafner, J. Phys. Condens. Matter 6 (1994) 8245.
[40] B. Hammer, L. Hansen, J.K. Norskov, T.U.o. Denmark, Lyngby, 1995.
[41] A.M. Goda, M.A. Barteau, J.G. Chen, J. Phys. Chem. B 110 (2006) 11823.
[42] B. Hammer, J.K. Norskov, Surf. Sci. 343 (1995) 211.
[43] M. Saeys, M.F. Reyniers, M. Neurock, G.B. Marin, Surf. Sci. 600 (2006) 3121.
[44] M.B. Zellner, J.G. Chen, J. Catal. 235 (2005) 393.